Environmental Science and Pollution Research (2023) 30:33795–33807
https://doi.org/10.1007/s11356-022-24646-6

RESEARCH ARTICLE

Enhanced persulfate activation by nitrogen-doped mesoporous carbon for efficiently degrading organic matters

Yueling Yu[1] · Jia Yang[1] · Xinfei Fan[1] · Yanming Liu[2]

Received: 4 June 2022 / Accepted: 4 December 2022 / Published online: 10 December 2022
© The Author(s), under exclusive licence to Springer-Verlag GmbH Germany, part of Springer Nature 2022

Abstract

Nitrogen-doped carbon materials (NMC) are widely used in peroxymonosulfate-based advanced oxidation processes (PMS-AOPs). Despite great efforts to improve the specific surface area of and the content of N atoms in catalysts for enhancing catalytic performance, this does not mean that the catalytic performance will improve with the increasing specific surface area and nitrogen content. Therefore, it is the key to optimize pore structure of NMC for maximizing the catalytic performance of nitrogen active sites. Herein, we synthesized the NMC as an efficient catalyst to activate PMS for the phenol removal. It can be found that the mesopore structure significantly accelerated the diffusion of reactants and might build the spatial confinement effect to improve the utilization of short life free radicals for further improving the removal efficiency. The removal efficiency of 1NMC750 (95%) with abundant mesopore channels was much higher than that of 1NMC750-0F127 (20%) with abundant micropore channels. Furthermore, the mechanism was confirmed to be radical ($SO_4^{\bullet-}$, •OH) and non-radical ($^1O_2$, electron transfer) pathways. This study proposed a new insight for improving the catalytic performance of carbon materials by coordinating the pore structure.

Keywords Nitrogen-doped carbon · Mesopore channel · Heterogeneous catalysis · Peroxymonosulfate · Reactive oxygen species · Oxidation mechanism

Introduction

The universal presence of refractory organic pollutants in wastewater has caused several environmental problems and posed threat to human health due to their biological toxicity and high persistence in the environment (Li et al. 2019). Various effective water remediation techniques (e.g., membrane separation, biodegradation, adsorption methods, and advanced oxidation process (AOP)) have been developed for the wastewater remediation (Zhu et al. 2021). Due to the merits of high efficiency and non-selectivity, AOP has been extensively studied to generate reactive oxygen species (ROS) to decompose organic matters (Wang et al. 2022b). In particular, sulfate radical ($SO_4^{\bullet-}$)–based AOP can generate $SO_4^{\bullet-}$ with strong oxidative capacity. Compared to classical hydroxyl radical (•OH), $SO_4^{\bullet-}$ possesses an equal or even higher oxidative potential ($SO_4^{\bullet-}$ ($E_0 = 2.5 \sim 3.1$ V) ≥ •OH ($E_0 = 1.9 \sim 2.7$ V)) and a longer lifespan ($SO_4^{\bullet-}$: 30–40 μs > •OH: 10^{-3} μs) (Xu et al. 2022). However, peroxymonosulfate (PMS) cannot generate ROS by self-activation without external catalyst activation due to its stable property (Wang and Wang 2018). In this regard, it is urgently to rationally design a high efficiency, green, and structurally stable PMS-AOP catalyst.

Nitrogen-doped carbons with the well-developed porosity and high surface area have been considered as the efficient PMS catalyst (de Andrade et al. 2020; Tian et al. 2022). Thereinto, the different types of nitrogen functional group may generate distinct catalytic property. The pyridinic N enhanced the catalytic performance by structuring the localized states (Ren et al. 2022). The pyrrolic N devoted two electrons to form the Lewis basic sites, resulting in the enhanced adsorption capacity of persulfate and

Responsible Editor: Ricardo A. Torres-Palma

✉ Xinfei Fan
fxf0909@dlmu.edu.cn

[1] College of Environmental Science and Engineering, Dalian Maritime University, No. 1 Linghai Road, Dalian, People's Republic of China 116026

[2] Key Laboratory of Industrial Ecology and Environmental Engineering (Ministry of Education, China), School of Environmental Science and Technology, Dalian University of Technology, Dalian 116024, China

pollutants (Chen et al. 2018). Moreover, the graphitic N can generate the more positive charged of the adjacent C atom, which was conducive to activate PMS (Duan et al. 2015b). The nitrogen-doped carbon materials can overcome the inevitable metal leaching and scarcity issues of metal-based catalyst (El Fakir et al. 2022). Tian et al. (2022) reported that nitrogen-doped porous carbon showed the enhanced catalytic capacity and adsorption capacity compared with that of original porous carbon. The original carbon material without doping nitrogen mainly relied on adsorption for removing phenol, while nitrogen-doped carbon showed great PMS activation capacity for efficient removal phenol (Wan et al. 2022). Despite many advances in developing nitrogen-doped carbon catalysts, most past studies have focused on the design and synthesis of novel nitrogen-doped carbon catalysts to enlarge surface area or insert more N atoms to improve catalytic performance (Ma et al. 2019). However, it is worth noting that the increasing surface area and nitrogen content may not mean improved catalytic capacity. The N atoms insert in different scaled pore channels (macropore, mesopore, and micropore) might also generate different catalytic performance (Liu et al. 2020b). Thereinto, mesopore is more conducive to enhance the reactant diffusion than micropore. Compared with macropore, mesopore possesses a larger specific surface area which is beneficial for the distribution of N active sites (Jiang et al. 2016). Moreover, recent studies have reported that mesopore channel can build the spatial confinement effect, restricting the pollutant molecules and short-lived active species in the nanoscale space. By constructing mesopore channels, the nanoscale spatial confinement can be generated for improving the pollutant degradation efficiency (Zhang et al. 2020). Consequently, nitrogen-doped mesoporous carbon has attracted extensive attention as a catalyst.

Based on the above innovations, nitrogen-doped mesoporous carbon was successfully fabricated through the soft-template self-synthesized method by using dicyandiamide (DCDA) as nitrogen source. The obtained nitrogen-doped mesoporous carbons were systematically characterized by scanning electron microscopy (SEM), X-ray photoelectron spectroscopy (XPS), Raman, and N_2 adsorption/desorption isotherms. The degradation efficiency of 1NMC750/PMS system (the system of 1NMC750 activated PMS) was examined in different reaction conditions (different pH and PMS dosage, the presence of different inorganic anions (Cl^-, HCO_3^-) and humic acid (HA)). Moreover, degradation experiments toward other pollutants manifest the versatility of 1NMC750/PMS system. The catalytic degradation mechanism of 1NMC750/PMS system was determined through the combination of radical quenching experiments, electron paramagnetic resonance (EPR), and electrochemical tests.

Materials and characterization

Reagents

Materials were presented in the Supporting information Text. S1.

Characterization

The morphologies of materials were observed by scanning electron microscopy (SEM, Hitachi S-4800) tests. X-ray photoelectron spectra (XPS) were conducted to analyze the elemental content. Raman spectra were obtained using Horiba Scientific LabRAM HR Evolution with a green laser at 532 nm. The specific surface area and pore size distribution were analyzed by N_2 adsorption/desorption measurements.

Synthesis of nitrogen-doped mesoporous carbon

The mesoporous carbon (MC) was obtained by soft-template self-synthesized method using the Pluronic F127 (F127) as the mesoporous structure-direct agent. Firstly, 0.378 g of F127 was dissolved in the solution of 1.74 g deionized water, 0.06 mL HCl (5 mol L^{-1}), and 2.3 g ethanol (EtOH). Then, 0.487-g triethyl orthoacetate and 0.541 g formaldehyde were added to the above mixture solution in turn, and stirred at 30 °C. After stirred for 20 min, 0 g, 0.039 g, 0.078 g, and 0.156 g dicyandiamide (DCDA) as the nitrogen source were added to solution and continued to stir for 30 min and named as the MC, 1NMC, 2NMC, and 3NMC, respectively. Following that, the resultant solutions were added to watch-glass and heated at 90 °C for 5 h in oven. The resultant deposits were carbonized under nitrogen atmosphere (650–950 °C for 3 h, 1 °C min^{-1}). In addition, sample carbonized at 750 °C without the use of the mesoporous structure agents of F127 was named as 1NMC750-0F127.

Experimental procedures and analytical methods

The both catalytic degradation and adsorption experiments were all carried out in the glass flask on the magnetic stirrers with a speed of 600 rpm. In the catalytic degradation experiments, the glass flask with a 50-mL mixture solution (pH = 6) of carbon catalyst (0.4 g/L), phenol solution (70 mg/L), and PMS oxidant (1.5 mM). After a certain interval, 0.3-mL sample was withdrawn, and a certain amount of methanol (MeOH) was immediately added to quench the residue radicals. After that, the solid catalyst was filtered with the 0.22-μm filter membrane. For the stability tests, the catalyst was collected after each cycle experiment by

filtration, followed by washing with copious amounts of EtOH and water and drying in oven. The detailed pollutants concentration analysis was shown in Table S1.

Results and discussion

Properties of catalyst

The morphological information of 1NMC750, as shown in SEM photos (Fig. 1a, b, and c), exhibiting some irregular multiple pore structure, which may derive from pyrolysis removal of template (F127). The Raman spectra (Fig. 1d) exhibited the degree of graphitization of carbon materials. The characteristic peaks were at around 1350 cm^{-1} and 1585 cm^{-1}, which were attributed to the appearance of defected (D) and graphite structures (G) (Wang et al. 2020). I_D/I_G value of 1NMC750 was 0.84, indicating the partial graphitization of 1NMC750 (Tian et al. 2022). The structural property of carbon material was assessed by the N_2 adsorption–desorption method (Fig. 1e), the characteristic of type IV isotherm and type I isotherm was observed in 1NMC750 and 1NMC750-0F127, respectively, suggesting mesopore and micropore was the main pore structure in 1NMC750 and 1NMC750-0F127 (Liu et al. 2020a; Thommes et al. 2015; Wang et al. 2021). Moreover, 1NMC750 contained a pore volume of 0.62 cm^3/g and an average pore size of 4.38 nm (Table S2). XPS results of carbon materials were conducted to investigate the chemical composition. As shown in Fig. 1f, the distinct peaks included C 1 s (284.8 eV), O 1 s (533 eV), and N 1 s (401.1 eV). Moreover, the high resolution of XPS N 1 s peaks (Fig. 1g) can be deconvoluted into four peaks at 398.7, 400.2, 401.2, and 403.8 eV, which corresponded to pyridinic N, pyrrolic N, graphitic N, and oxidated N, respectively (Huang et al. 2021). Thereinto, the pyridinic N and graphitic N were the active center for PMS activation to generate $^1O_2$ (Wan et al. 2022). The pyrrolic N was reported in the previous studies that had a promoting effect on the pollutant adsorption (Zhong et al. 2021). Therefore, the above results suggested that the nitrogen mesoporous carbon may have good catalytic potential.

Degradation performance in different systems

By degrading phenol in different catalytic degradation systems, the catalytic performance of the nitrogen doped mesoporous carbon for PMS activation was confirmed. The removal efficiency of phenol was merely 49% in the 1NMC750 system (Fig. 2a and b). Since 1NMC750 had the BET surface area of 627.44 $m^2\ g^{-1}$ (Table S2), the 1NMC750 possessed the excellent adsorption capacity, thus resulting in the removal of phenol in the 1NMC750 system. The phenol degradation efficiency with PMS alone was approximately 5% with the pseudo-first order kinetics constant (k) of 0.0002 min^{-1}. Notably, the removal rate exhibited an outstanding enhancement and achieved at 95% (0.0192 min^{-1}) with the coexistence of PMS and 1NMC750. The above results revealed that the degradation performance of 1NMC750/PMS system far outweighs that of PMS alone and 1NMC750 alone. As shown in Fig. S1, the PMS decomposition results also corroborated the negligible self-activation of PMS (10%). By contrast, the decomposition rate of PMS was as high as 80% with the existent of 1NMC750, suggesting the excellent catalytic performance of 1NMC750. The above results demonstrated that PMS had the feeble oxidation capacity and was difficult to be decomposed without external activations (Fan et al. 2020; Zhong et al. 2021). Compared with PMS alone and 1NMC750 alone, 1NMC750/PMS system demonstrated an increment in phenol degradation, which can be ascribed to the high PMS decomposition rate in the 1NMC750/PMS system, resulting in the generation of ROS.

In order to explore the catalytic relationship between the active sites of nitrogen atoms and the mesopore structure, the 1NMC750-0F127 as a control was fabricated without the addition of F127. The removal rate of 1NMC750-0F127/PMS system decreased obviously (20%) compared with 1NMC750/PMS system. As listed in Table S2, the volume ratio (V_{mic}/V_{total}) of 1NMC750-0F127 was 0.94, indicating the pore structure of 1NMC750-0F127 was constituted by micropore structure, which leaded to the fact that the nitrogen atoms can only distribute in the micropores. Moreover, the volume ratio (V_{mic}/V_{total}) of 1NMC750 decreased to 0.29, proving the dominated role of mesopore structure in 1NMC750. Therefore, the enhanced catalytic performance of 1NMC750 could be attributed to the mesoporous structure effect, which can make the spatial confinement effect to shorten migration distance among ROS, pollutants, and active sites (Duan et al. 2015a).

Catalyst optimization

The catalytic degradation performance of mesoporous carbon with different N doping content was evaluated, and thus, the addition of nitrogen source (DCDA = 0 g, 0.039 g, 0.078 g, 0.156 g, corresponded to MC750, 1NMC750, 2NMC750, 3NMC750) was changed in the fabrication preparation process. XPS analysis (Fig. 3a) revealed the N content of MC750, 1NMC750, 2NMC750, and 3NMC750 were 0, 1.50, 2.62, and 3.83 at%, respectively. During catalytic oxidation processes (Fig. 3b), 1NMC750 presented much higher phenol removal efficiency (95%) than that of MC750 (33%), 2NMC750 (59%), and 3NMC750 (50%) under the same conditions. The kinetic rate constant on 1NMC750 (0.0192 min^{-1}) was 6–12 times greater than those on MC750, 2NMC750, and 3NMC750. It was worth noting

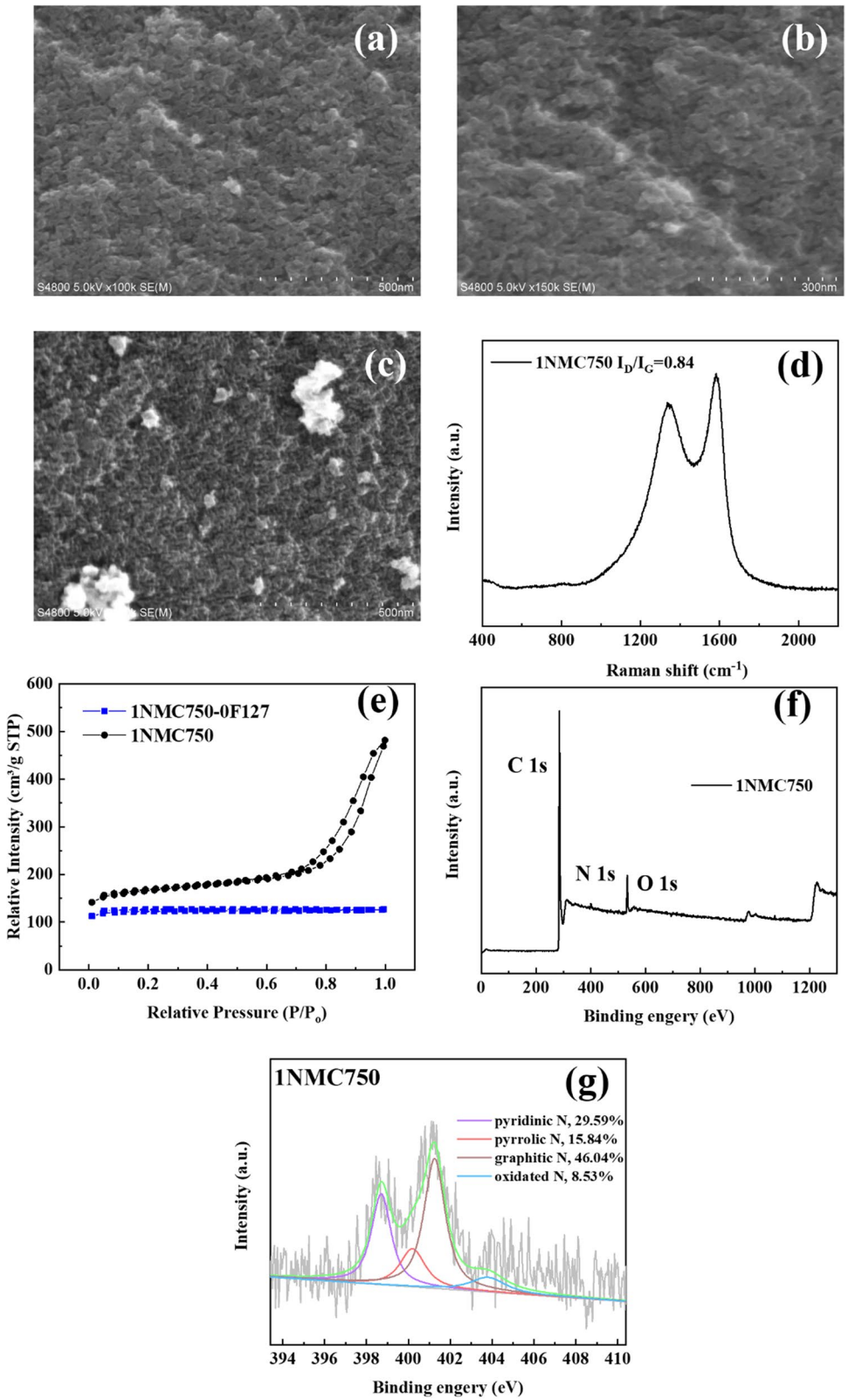

Fig. 1 SEM image of 1NMC750 (**a**, **b**, and **c**); Raman spectra (**d**); N_2 adsorption–desorption isotherms of 1NMC750 and 1NMC750-0F127 (**e**); XPS spectra of 1NMC750 (**f**) and (**g**)

that nitrogen doping can improve the catalytic degradation capacity of the catalyst. As shown in Fig. S4, only 31% target pollutant was removed within 90 min by MC750 alone, while the removal efficiency of 1NMC750 alone increased to 49%, indicating that the nitrogen functional groups played an important role in the adsorption process. The abundant

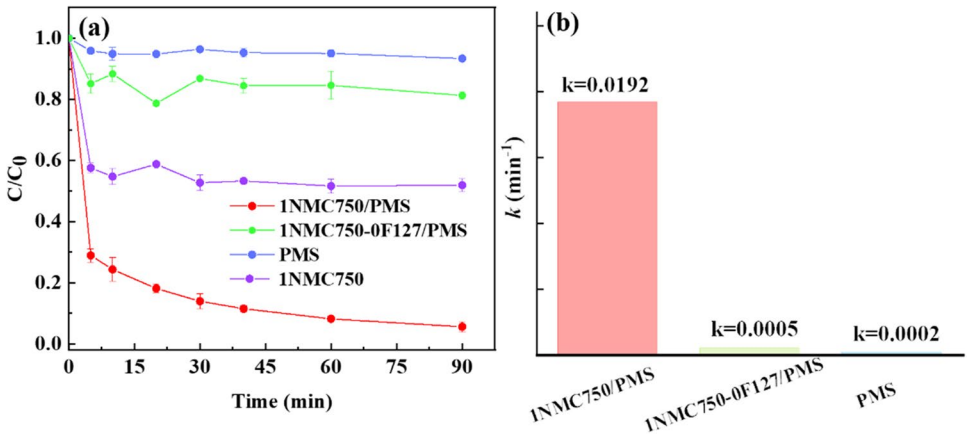

Fig. 2 Phenol degradation performance (**a**) and *k* value (**b**) in different systems

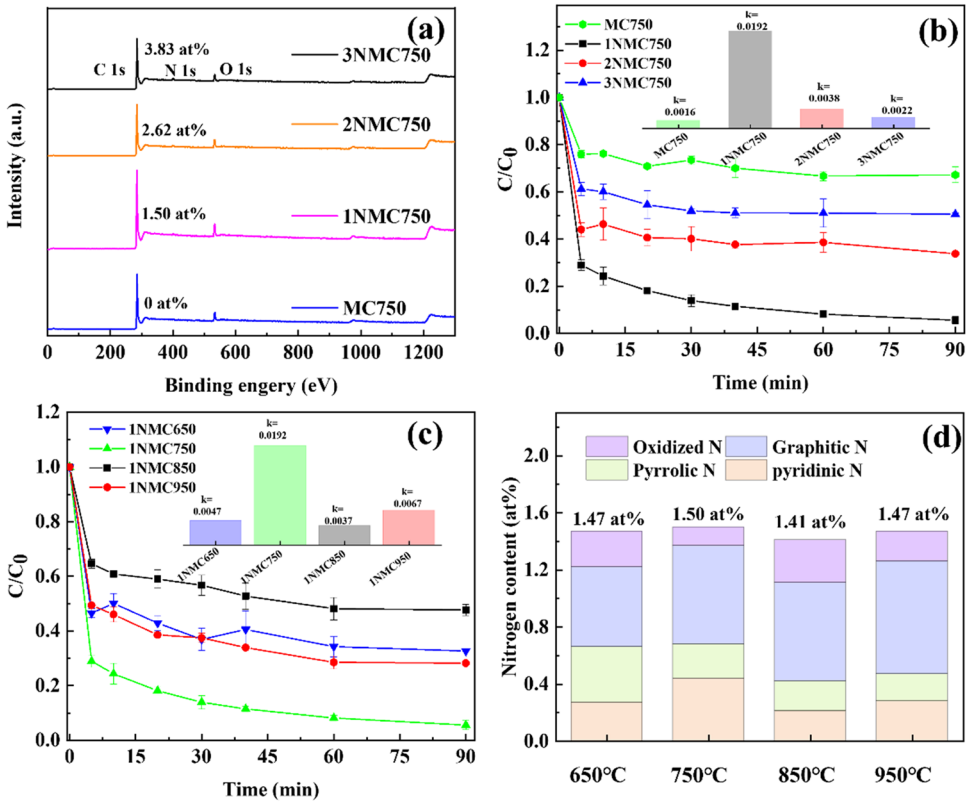

Fig. 3 XPS spectra of catalysts with different amount of doped N (**a**); Phenol degradation performance in presence of different amount of N doped mesoporous carbon (**b**), and in presence of different pyrolysis temperature of 1NMC (**c**); Contents of four nitrogen species in 1NMC under different pyrolysis temperatures (**d**)

adsorption sites of 1NMC750 can promote the accumulation of PMS and pollutants. Moreover, the removal efficiency of the MC750 alone and MC750/PMS system exhibited negligible difference (Fig. 3b and Fig. S4), suggesting that the samples without N functional groups may not activate PMS even if the presence of oxygen functional groups. However, the adsorption capacity and catalytic degradation capacity was not completely related to the doping amount of nitrogen functional groups. Such case can be attributed that the introduction of excess nitrogen source into carbon may cause the collapse of carbon skeleton and disturb the charge, resulting in pore structural collapse and the reduced exposure of active sites (Ding et al. 2020). These above results suggested that 0.039-g DCDA was the most desirable doping amount for fabricating catalyst to activate PMS toward the phenol degradation. Moreover, it was important to select an optimal pyrolysis temperature to prepare catalyst for subsequent experiments. Therefore, the effect of pyrolysis temperature on the catalytic properties of carbon materials was also evaluated. As illustrated in Fig. 3c, phenol removal rate increased gradually as the pyrolysis temperature increasing from 650 to 750 °C. A low removal efficiency of 53% was achieved at pyrolysis temperature of 850 °C. To continue raising the pyrolysis temperature to 950 °C, the removal rate

had a slight increase to 78%. The kinetic rate constant for phenol oxidation on 1NMC750 was 2–4 times greater than those on 1NMC650, 1NMC850, and 1NMC950. Therefore, the optimal pyrolysis temperature of 750 °C was selected for subsequent experiments in this work. Previous studies have shown that the change of pyrolysis temperature can lead to the variation of surface characteristics and the catalytic performance would change accordingly (Li et al. 2020a). Therefore, the XPS spectra of surface element analysis of carbon-based materials under different pyrolysis temperatures were shown in Fig. 1g and Fig. S2. The relative contents of each N species in the carbon samples are shown in Fig. 3d and Table S3. A positive correlation was found between pyridinic N and *k*, implying that pyridinic N was in favor of PMS activation (Fig. S3). Moreover, the adsorption performance was up with the increasing content of pyridinic N (Table S3), indicating that the pyridinic N can also promote the pollutant adsorption, and thus increasing the contact between the pollutant, catalyst, and PMS under catalytic process.

Phenol degradation in different conditions

The dosage of PMS was an important influencing factor of the amount of reactive oxygen species (ROS) and thus was investigated in Fig. 4a. The phenol removal efficiency increased from 70 to 95% when PMS concentration was increased from 0.5 to 1.5 mM. However, when the PMS concentration increased to 2.0 mM, the phenol degradation efficiency decreased to 83%. With the addition of the higher concentration of PMS, a large number of ROS would be generated through the catalyst activation, which could effectively attack pollutants, thus improving the speed of catalytic reaction (Liu et al. 2020a). The increase of PMS concentration leaded to the gradual increase of radical concentration until exceeding the optimal range, and induced self-scavenging reactions (Kang et al. 2016). Thus, 1.5 mM was used as the optimal PMS concentration. Generally, catalytic performance in catalytic process of carbon-based catalyst was susceptible to the solution pH (Zuo et al. 2022), and thus, different initial pH was selected to investigate the phenol removal efficiency. It was shown (Fig. 4b) that the phenol removal was 85%, 95%, and 92% under the pH of 2, 6, and 8 respectively, with the kinetic rate constant of 0.0102 min^{-1}, 0.0192 min^{-1}, and 0.0114 min^{-1}. The removal efficiency under acidic condition was generally worse than that of under neutral and alkaline solution, because of the quencher reaction between the H^+ and ROS (•OH and $SO_4^{\bullet-}$) (Wang et al. 2017). Mushtaque Ahmad et al. have reported that PMS could be activated by base in the high alkaline solution (Ahmad et al. 2013). Therefore, the solution pH value in the experimental condition was controlled at pH < 9 to rule out the influence of base activation. Therefore, pH = 6 was selected as the optimal condition for the following experiments. In order to evaluate the adaptability of NMC750/PMS system, the inhibition of inorganic anions and natural organic matter (NOM) on phenol degradation was investigated (Zhao et al. 2017). The degradation efficiency of phenol decreased slightly with the presence of Cl^- (Fig. 4c). Cl^- can react with •OH and $SO_4^{\bullet-}$ to produce lower oxidation potential radicals as shown in Eqs. (1), (2), (3), and (4) (Li et al. 2020b). Therefore, the ROS was consumed rapidly by the added Cl^-, resulting in the reduction of pollutant removal rate. Compared with Cl^-, the degradation efficiency decreased significantly with the present of HCO_3^-, which can be ascribed to the reaction between HCO_3^- and $O_2^{\cdot-}$ (Wang et al. 2018) and therefore inhibited the formation of $^1O_2$ in the reaction solution. Consequently, the present of HCO_3^- can lead to the reduction of $^1O_2$ (Eqs. (5), (6), and (7)) (Pang et al. 2022). Moreover, HA had a significant inhibitory effect on the degradation of phenol in the 1NMC750/PMS system (Fig. 4e). Such case was because the hydrogen bond interaction enhanced the adsorption of HA and then occupied the active sites of catalysts. Moreover, HA can be acted as another pollutant that competed with the target pollutant to reduce the utilization of radicals and other oxidizing species (de Andrade et al. 2020).

$$SO_4^{\cdot-} + Cl^- \rightarrow SO_4^{2-} + Cl^{\cdot} \quad (1)$$

$$\cdot OH + Cl\cdot \rightarrow ClOH^{\cdot-} \quad (2)$$

$$ClOH^{\cdot-} + H^+ \rightarrow Cl^{\cdot} + H_2O \quad (3)$$

$$Cl^{\cdot} + Cl^- \rightarrow Cl_2^{\cdot-} \quad (4)$$

$$HCO_3^- \rightarrow CO_3^{2-} + H^+ \quad (5)$$

$$CO_3^{2-} + O_2^{\cdot-} \rightarrow \cdot CO_3^- + O_2^{2-} \quad (6)$$

$$\cdot CO_3^- + O_2^{\cdot-} \rightarrow \cdot CO_3^{2-} + O_2 \quad (7)$$

Identification of radicals

ROS played a vital role in the 1NMC750/PMS system for efficient degradation of organic pollutants (Xu et al. 2022). The possible oxidative pathway generated from catalyst activation include •OH and $SO_4^{\bullet-}$, $^1O_2$, and electron transfer. Therefore, radical quenching experiments were performed to identify radicals in 1NMC750/PMS system. In general, MeOH was used as the quencher of both $SO_4^{\bullet-}$ and •OH (Guan et al. 2011). Moreover, TBA was employed to scavenge •OH (Tang et al. 2018). As can be seen from

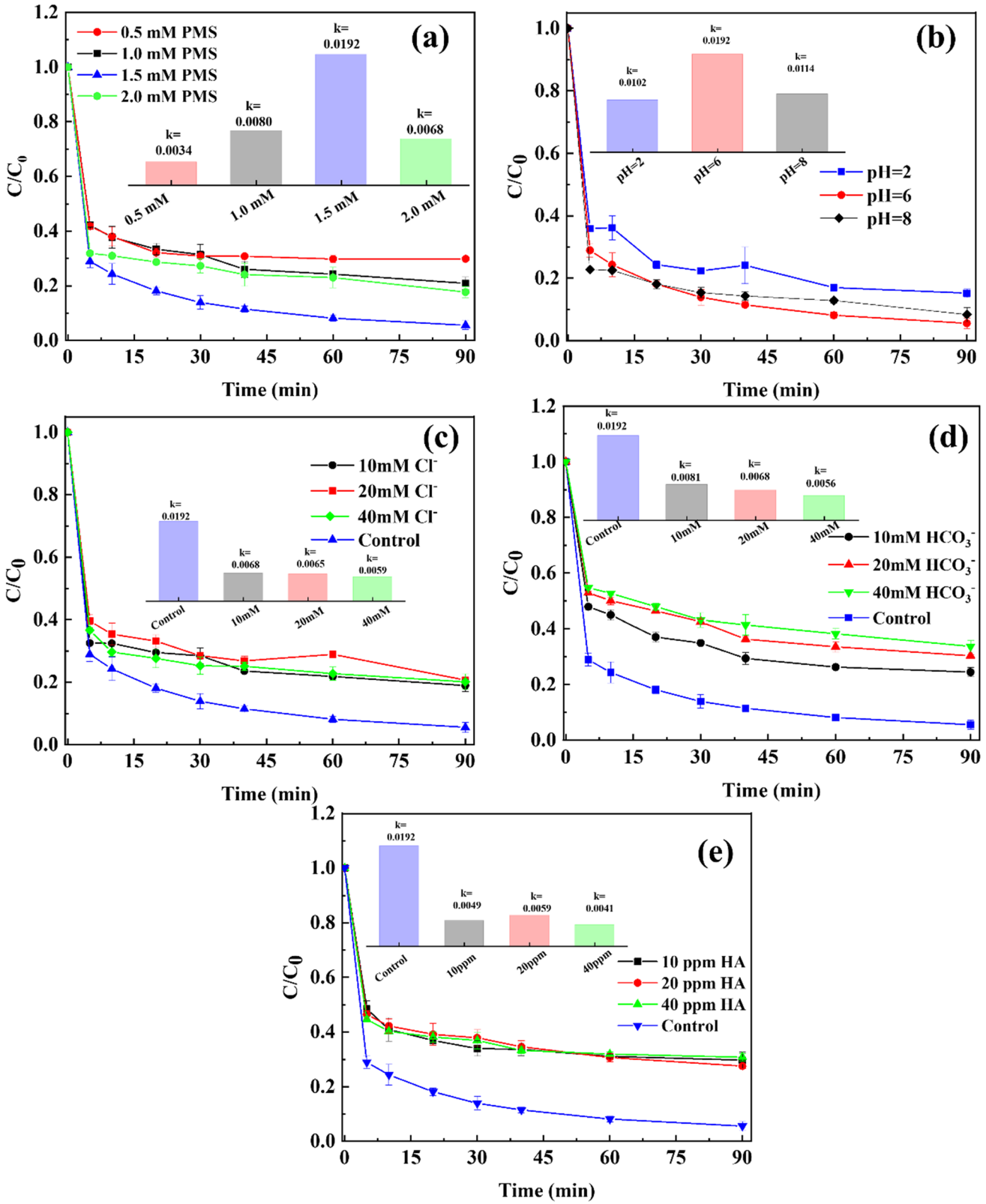

Fig. 4 Effect of PMS dosage (**a**), pH (**b**) different concentration of Cl^- (**c**) and HCO_3^- (**d**), and different concentration of HA (**e**)

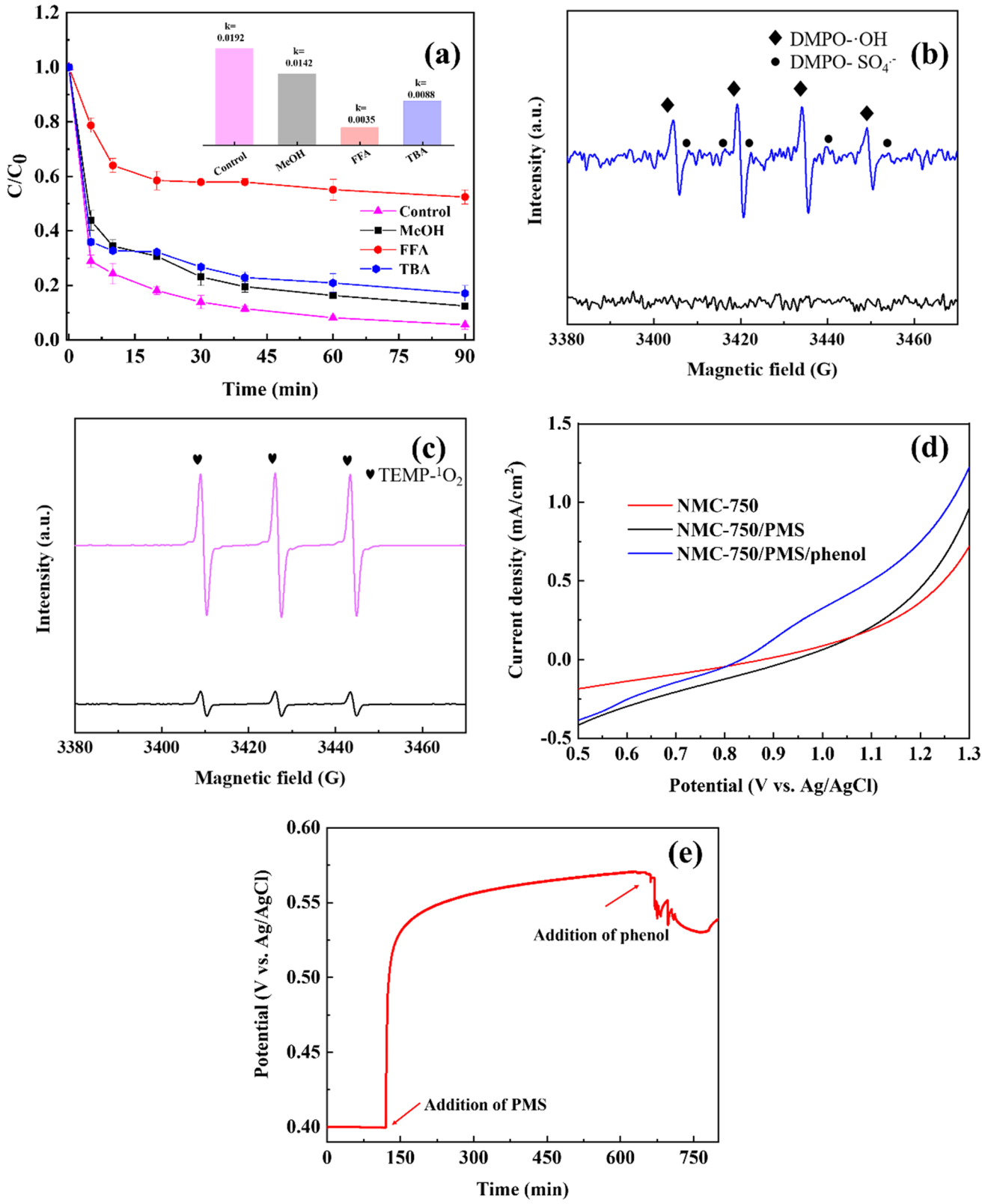

Fig. 5 Degradation performance and corresponding reaction rate constant of phenol degradation with different quenchers (**a**); EPR spectra (**b**) and (**c**); LSV in different systems (**d**); open circuit potential (OCP) (**e**)

Fig. 5a, when MeOH and TBA existed in the 1NMC750/PMS system, the phenol degradation efficiency decreased to 87% and 83% along with the decrease of *k* from 0.0192 to 0.0142 min^{-1} and 0.0088 min^{-1}. Unexpectedly, the inhibitory of TBA on phenol oxidation degradation efficiency was slightly higher than that of MeOH. The above anomalous results have been reported in the previous study (Liang et al. 2013), which can be ascribed to the lower dielectric constant of TBA (12.5) than MeOH (33.7). Thus, TBA was more readily accessible to catalyst surface, which can occupy active sites on the surface of catalyst and react with its surface ROS. Therefore, compared with MeOH, TBA had a stronger inhibitory effect on phenol degradation. The above results suggested that •OH and $SO_4^{\bullet-}$ may be generated in this solution, and therefore, the types of ROS needed to be further confirmed. Therefore, EPR experiments were performed to further identify the radicals involved in the 1NMC750/PMS system. The DMPO was used as the effective radical trapping agent of •OH and $SO_4^{\bullet-}$. As shown in Fig. 5b, the signal of DMPO-•OH and DMPO-$SO_4^{\bullet-}$ were observed in the reaction process, demonstrating the present of •OH and $SO_4^{\bullet-}$. Expect radical pathway, non-radical pathway may also participate in the phenol degradation, and FFA was chosen as the quencher of $^1O_2$ (Fig. 5a). It was worth noting that the removal rate drastically reduced to 48% with the addition of FFA, indicating the $^1O_2$ may be the main degradation factor in the 1NMC750/PMS system. In addition, Fig. 5c clearly revealed a more significant 1:1:1 triplet characteristic signal of TEMP-$^1O_2$ in the 1NMC750/PMS system than that of in the PMS alone system, further affirming that $^1O_2$ was indeed generated in the 1NMC750/PMS system. Electron transfer can also provide an additional non-radical pathway in the carbon catalyst/PMS system. Electrochemical measurements (linear sweep voltammetry, LSV; open circuit potential, OCP) were utilized to investigate the electron transfer in the NMC750/PMS system. In electrochemical measurements, the 1NMC750 catalyst-modified glassy carbon (GC) was working electrode, and Ag/AgCl was reference electrode, and Pt tablet was counter electrode. The LSV currents of 1NMC750/PMS/phenol, 1NMC750/PMS, and 1NMC750 alone were recorded and can be observed in Fig. 5d. The current density increased with the added of PMS and was higher than that of 1NMC750 alone. Compared with the 1NMC750/PMS system, the current density increased significantly when 1NMC750, PMS, and phenol were present. This was strong evidence that electron transfer generated in the 1NMC750/PMS/phenol system. To further prove the present of electron transfer, the OCP was conducted. As shown in the OCP model (Fig. 5e), the potential increased rapidly in the presence of PMS in solution. Whereas, when phenol was added in the solution, the potential began to fall sharply, indicating the generation of the electron transfer process. Therefore, the electron transfer process also participated in the catalytic oxidation. Based on the above quenching degradation results, non-radical pathway may be more predominant than radical pathway, while radical pathway also played an important role in accelerating the reaction. Therefore, it can further prove that the moderate suppressed effect of Cl^- was because •OH and $SO_4^{\bullet-}$ was not the main oxidant species responsible for phenol degradation. And a significant decrease in removal efficiency was generated in the present of HCO_3^-. Thereinto, HCO_3^- had a significant inhibitory on the generation of $^1O_2$, in which $^1O_2$ was the dominant ROS in the 1NMC750/PMS system.

Reusability of catalyst and active sites identification

Catalyst reusability is a crucial influence to consider the actual applicability. Therefore, the reusability experiments of 1NMC750 were conducted in this work (Fig. 6a). Along with the increase cycle of catalytic degradation, phenol removal rate decreased from 95% in first cycle to almost 71% in second cycle and 45% in third cycle. To analyze the reasons of catalyst deactivation, BET surface area and surface functional groups of the catalyst before and after the reaction were characterized. Figure 6b depicted the N 1 s spectra of 1NMC750 obtained after the second degradation cycle, while the proportion of pyrrolic N and graphitic N in the N content of the used 1NMC750 were negligible changed compared with that of before activation. However, the proportion of pyridinic N exhibited a significant downward trend from 29.59% (before oxidation process) to 18.50% (after oxidation process). By contrast, the oxidized N increased from 8.53 to 22.50%. The above results could be ascribed to the conversion of pyridinic N to oxidized N, indicating the pyridinic N was the active site in the phenol oxidation process, and the results were consistent with the correlation analysis of nitrogen in different pyrolysis temperatures (the "Catalyst optimization" section). Therefore, the deactivation reason can be attributed to the consumption of active sites of 1NMC750 (Guo et al. 2017; Sun et al. 2021; Tian et al. 2022). Moreover, the loss of BET surface area may also be a factor affecting catalytic performance. Therefore, the N_2 adsorption/desorption isotherms of used 1NMC750 was conducted (Table S2). Compared with the raw 1NMC750, the BET surface area of used 1NMC750 decreased obviously, indicating the consumption of BET surface area in the catalytic degradation process. During the catalytic degradation process, the PMS and target pollutant molecules were adsorbed in the pore channel of 1NMC750 rapidly, which could speed up the catalytic degradation reaction. Moreover, the degradation intermediates accumulated on the catalyst during the catalytic reaction, resulting in a decrease in the BET surface area. After catalytic reaction, original pore structure was devastated and combined into a bigger pore structure due to a large number of adsorption pollutants into

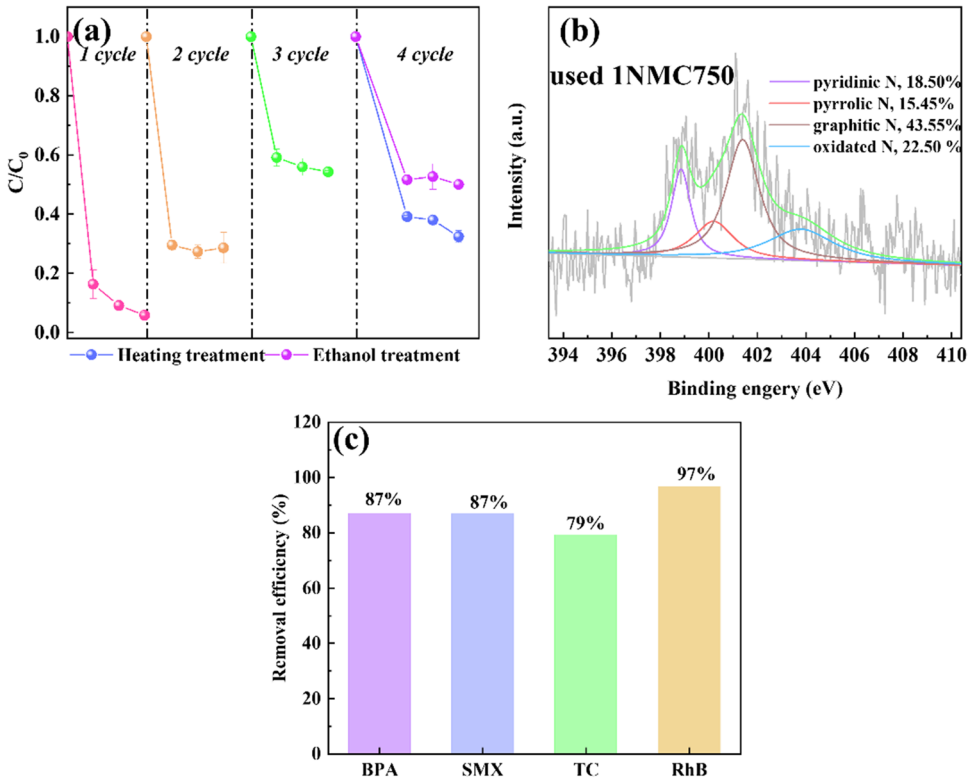

Fig. 6 Reusability of 1NMC750 (**a**); XPS spectra for used 1NMC750 (**b**); the degradation efficiency of different pollutants (**c**)

the pore channel. Thus, the used 1NMC750 had a larger pore diameter (used 1NMC750 (13.73 nm) > raw 1NMC750 (4.38 nm)) and a smaller pore volume (used 1NMC750 (0.25 $cm^3\ g^{-1}$) < raw 1NMC750 (0.62 $cm^3\ g^{-1}$)) than raw 1NMC750. Therefore, the catalyst needed to be regenerated for the next catalytic degradation process. For the regeneration of catalyst, the used catalyst was immersed in the ethanol solution for hydrogenation under mild conditions, which may remove the adsorbed intermediates for restoring the activity of the catalyst. However, the catalytic performance of 1NMC750 merely recovered to 50% after immersing in ethanol solution for 2 h. It was worth noting that the catalytic degradation capacity of 1NMC750 recovered to 67% under calcining at 750 °C for 1 h under argon flow. It can be ascribed to the decomposition of intermediates through pyrolysis process and the exposure of active sites (Pang et al. 2022).

Degradation test toward other pollutants

The 1NMC750/PMS system was further tested to assess catalytic performance for the removal of various recalcitrant organic pollutants generated from industrial and pharmaceutical applications, including sulfamethoxazole (SMX), tetracycline (TC), bisphenol A (BPA), and rhodamine B (RhB). As shown in Fig. 6c, the removal efficiencies in 1NMC750/PMS system of 97%, 87%, 87%, and 80% were obtained for RhB, BPA, SMX, and TC, respectively. 1NMC750/PMS system had the high removal efficiency of various organic contaminants. Therefore, the 1NMC750/PMS system had the universal applicability for various refractory pollutants.

Activation mechanism

On the basis of aforementioned results, the possible activation mechanism in 1NMC750/PMS system was proposed in Fig. 7. Firstly, assisted by the abundant mesoporous structure of 1NMC750, PMS was readily adsorbed in the porous channel and onto the catalyst surface. Then, pyridinic N serve as active sites can accelerate the nucleophilic addition reaction to generate $^1O_2$ (Eqs. 8 and 9) and promote the adsorbed PMS decompose into $^1O_2$ (Eq. 10) (Wan et al. 2022). Moreover, the graphitic N can extract electrons from the adsorbed PMS and produce radicals (Eqs. 11 and 12) (Wang et al. 2022a). When abundant PMS molecules adsorbed onto the nitrogen-doped carbon, the electron-rich phenol as the electron donor transported electron to PMS and then was directly attacked by the activated PMS (Eqs. 13 and 14) (Zhang et al. 2021).

$$HSO_5^- \rightarrow SO_5^{\cdot-} + H^+ + e^- \quad (8)$$

$$SO_5^{\cdot-} + SO_5^{\cdot-} \rightarrow 2SO_4^{2-} + {}^1O_2 \quad (9)$$

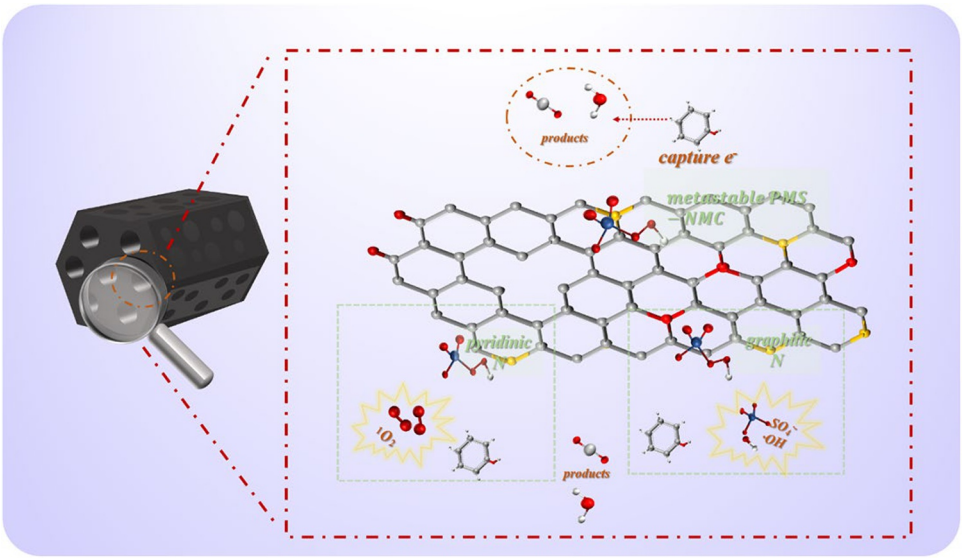

Fig. 7 Proposed mechanism of PMS activation by 1NMC750 for phenol degradation

$$HSO_5^- + SO_5^{2-} \rightarrow SO_4^{2-} + HSO_4^- + {}^1O_2 \quad (10)$$

$$HSO_5^- + e^- \rightarrow SO_4^{\cdot-} + OH^- \quad (11)$$

$$HSO_5^- + e^- \rightarrow SO_4^{2-} + \cdot OH \quad (12)$$

$$PMS + NMC \rightarrow metastablePMS - NMC \quad (13)$$

$$Phenol + metastablePMS - NMC \rightarrow products \quad (14)$$

Conclusion

In this study, the nitrogen-doped mesoporous carbon material was synthesized and used to activate PMS for phenol degradation. Due to the abundant mesopore structure in 1NMC750, the 1NMC750/PMS system had an outstanding phenol degradation efficiency, and its catalytic performance was higher than 1NMC750-0F127/PMS system. The radical quenching and EPR experiments as well as electrochemical analysis were conducted to confirm the present of radical ($SO_4^{\bullet-}$, •OH) and non-radical ($^1O_2$, electron transfer) pathway. Besides, the analysis results suggested that pyridinic N was likely to exist as main active sites. 1NMC750/PMS system exhibited not only excellent catalytic degradation performance toward phenol, but also had excellent removal efficiency rate to other contaminants. In short, this study provided a promising strategy for further optimize catalytic performance of metal-free carbon materials by regulating pore structures.

Supplementary Information The online version contains supplementary material available at https://doi.org/10.1007/s11356-022-24646-6.

Author contribution Yueling Yu: writing-original draft, conceptualization, methodology, investigation, Software. Jia Yang: data curation, investigation. Xinfei Fan: conceptualization, resources, funding acquisition, writing — review and editing. Yanming Liu: resources, funding acquisition, writing — review and editing.

Funding This work was supported by the National Natural Science Foundation of China (22076019), Xingliao talent program (XLYC2007069), the Natural Science Foundation of Liaoning Province (2021-MS-139), and the Innovation and Entrepreneurship Projects for High-level Talents in Dalian (2019RQ132).

Data availability The datasets used/ or analysed during the current study are available from the corresponding author on reasonable request.

Declarations

Ethics approval and consent to participate Not applicable.

Consent for publication All authors agree to publication in this journal.

Competing interests The authors declare no competing interests.

References

Ahmad M, Teel AL, Watts RJ (2013) Mechanism of persulfate activation by phenols. Environ Sci Technol 47(11):5864–5871

de Andrade JR, Vieira MGA, da Silva MGC and Wang SB (2020) Oxidative degradation of pharmaceutical losartan potassium with N-doped hierarchical porous carbon and peroxymonosulfate. Chem. Eng. J. 382

Chen X, Oh WD, Lim TT (2018) Graphene- and CNTs-based carbocatalysts in persulfates activation: material design and catalytic mechanisms. Chem Eng J 354:941–976

Ding DH, Yang SJ, Qian XY, Chen LW and Cai TM (2020) Nitrogen-doping positively whilst sulfur-doping negatively affect the catalytic activity of biochar for the degradation of organic contaminant. Appl. Catal. B Environ. 263

Duan XG, Sun HQ, Kang J, Wang YX, Indrawirawan S, Wang SB (2015a) Insights into heterogeneous catalysis of persulfate activation on dimensional-structured nanocarbons. ACS Catal 5(8):4629–4636

Duan XG, Sun HQ, Wang YX, Kang J, Wang SB (2015b) N-doping-induced nonradical reaction on single-walled carbon nanotubes for catalytic phenol oxidation. ACS Catal 5(2):553–559

El Fakir AA, Anfar Z, Enneiymy M, Jada A, El Alem N (2022) Conjugated polymers templated carbonization to design N, S co-doped finely tunable carbon for enhanced synergistic catalysis. Appl. Catal. B Environ. 300

Fan Y, Zhou ZY, Feng Y, Zhou Y, Wen L, Shih KM (2020) Degradation mechanisms of ofloxacin and cefazolin using peroxymonosulfate activated by reduced graphene oxide-$CoFe_2O_4$ composites. Chem. Eng. J. 383

Guan YH, Ma J, Li XC, Fang JY, Chen LW (2011) Influence of pH on the formation of sulfate and hydroxyl radicals in the UV/peroxymonosulfate system. Environ Sci Technol 45(21):9308–9314

Guo YP, Zeng ZQ, Li YL, Huang ZG, Yang JY (2017) Catalytic oxidation of 4-chlorophenol on in-situ sulfur-doped activated carbon with sulfate radicals. Sep Purif Technol 179:257–264

Huang YM, Li G, Li MZ, Yin JJ, Meng N, Zhang D, Cao XQ, Zhu FP, Chen M, Li L, Lyu XJ (2021) Kelp-derived N-doped biochar activated peroxymonosulfate for ofloxacin degradation. Sci. Total Environ. 754

Jiang TT, Wang Y, Wang K, Liang YR, Wu DC, Tsiakaras P, Song SQ (2016) A novel sulfur-nitrogen dual doped ordered mesoporous carbon electrocatalyst for efficient oxygen reduction reaction. Appl Catal B Environ 189:1–11

Kang J, Duan XG, Zhou L, Sun HQ, Tade MO, Wang SB (2016) Carbocatalytic activation of persulfate for removal of antibiotics in water solutions. Chem Eng J 288:399–405

Li J, Jiang J, Pang SY, Sun SF, Wang LH, Zhou Y, Wang Z, Gao Y (2019) A novel strategy using peroxymonosulfate to control the formation of iodinated aromatic products in treatment of phenolic compounds by permanganate. Environ. Sci.: Water Res. Technol. 5(9), 1515–1522

Li J, Zhu J, Fang L, Nie Y, Tian N, Tian X, Lu L, Zhou Z, Yang C, Li Y (2020a) Enhanced peroxymonosulfate activation by supported microporous carbon for degradation of tetracycline via non-radical mechanism. Sep. Purif. Technol. 240

Li WQ, Li SQ, Tang Y, Yang XL, Zhang WX, Zhang XD, Chai HX, Huang YM (2020b) Highly efficient activation of peroxymonosulfate by cobalt sulfide hollow nanospheres for fast ciprofloxacin degradation. J. Hazard. Mater. 389

Liang HY, Zhang YQ, Huang SB, Hussain I (2013) Oxidative degradation of p-chloroaniline by copper oxidate activated persulfate. Chem Eng J 218:384–391

Liu SY, Lai C, Li BS, Zhang C, Zhang MM, Huang DL, Qin L, Yi H, Liu XG, Huang FL, Zhou XR, Chen L (2020a) Role of radical and non-radical pathway in activating persulfate for degradation of p-nitrophenol by sulfur-doped ordered mesoporous carbon. Chem. Eng. J. 384

Liu WQ, Qi JW, Bai PY, Zhang WD, Xu L (2020b) Utilizing spatial confinement effect of N atoms in micropores of coal-based metal-free material for efficiently electrochemical reduction of carbon dioxide. Appl. Catal. B Environ. 272

Ma C, Hou PF, Wang XP, Wang Z, Li WT, Kang P (2019) Carbon nanotubes with rich pyridinic nitrogen for gas phase CO_2 electroreduction. Appl Catal B Environ 250:347–354

Pang KF, Sun W, Ye F, Yang LH, Pu MJ, Yang C, Zhang QC, Niu JF (2022) Sulfur-modified chitosan derived N,S-co-doped carbon as a bifunctional material for adsorption and catalytic degradation sulfamethoxazole by persulfate. J. Hazard. Mater. 424

Ren W, Cheng C, Shao PH, Luo XB, Zhang H, Wang SB, Duan XG (2022) Origins of electron-transfer regime in persulfate-based nonradical oxidation processes. Environ Sci Technol 56(1):78–97

Sun W, Pang KF, Ye F, Pu MJ, Zhou CZ, Huang HM, Zhang QC, Niu JF (2021) Carbonization of camphor sulfonic acid and melamine to N,S-co-doped carbon for sulfamethoxazole degradation via persulfate activation: nonradical dominant pathway. Sep. Purif. Technol. 279

Tang L, Liu YI, Wang JJ, Zeng GM, Deng YC, Dong HR, Feng HP, Wang JJ, Peng B (2018) Enhanced activation process of persulfate by mesoporous carbon for degradation of aqueous organic pollutants: electron transfer mechanism. Appl Catal B Environ 231:1–10

Thommes M, Kaneko K, Neimark AV, Olivier JP, Rodriguez-Reinoso F, Rouquerol J, Sing KSW (2015) Physisorption of gases, with special reference to the evaluation of surface area and pore size distribution (IUPAC Technical Report). Pure Appl Chem 87(9–10):1051–1069

Tian WJ, Lin JK, Zhang HY, Duan XG, Wang H, Sun HQ, Wang SB (2022) Kinetics and mechanism of synergistic adsorption and persulfate activation by N-doped porous carbon for antibiotics removals in single and binary solutions. J. Hazard. Mater. 423

Wan Y, Hu Y, Zhou WJ (2022) Catalytic mechanism of nitrogen-doped biochar under different pyrolysis temperatures: the crucial roles of nitrogen incorporation and carbon configuration. Sci. Total Environ. 816

Wang GL, Chen S, Quan X, Yu HT, Zhang YB (2017) Enhanced activation of peroxymonosulfate by nitrogen doped porous carbon for effective removal of organic pollutants. Carbon 115:730–739

Wang H, Wang H, Yan Q (2022a) Peroxymonosulfate activation by algal carbocatalyst for organic dye oxidation: insights into experimental and theoretical. Sci. Total Environ. 816

Wang J, Duan XG, Gao J, Shen Y, Feng XH, Yu ZJ, Tan XY, Liu SM, Wang SB (2020) Roles of structure defect, oxygen groups and heteroatom doping on carbon in nonradical oxidation of water contaminants. Water Res. 185

Wang JL, Wang SZ (2018) Activation of persulfate (PS) and peroxymonosulfate (PMS) and application for the degradation of emerging contaminants. Chem Eng J 334:1502–1517

Wang MM, Cui YK, Cao HY, Wei P, Chen C, Li XY, Xu J, Sheng GP (2021) Activating peroxydisulfate with Co_3O_4/$NiCo_2O_4$ double-shelled nanocages to selectively degrade bisphenol A - a nonradical oxidation process. Appl. Catal. B Environ. 282

Wang XH, Zhang P, Wang CP, Jia HZ, Shang XF, Tang JC, Sun HW (2022b) Metal-rich hyperaccumulator-derived biochar as an efficient persulfate activator: role of intrinsic metals (Fe, Mn and Zn) in regulating characteristics, performance and reaction mechanisms. J. Hazard. Mater. 424

Wang YB, Liu M, Zhao X, Cao D, Guo T, Yang B (2018) Insights into heterogeneous catalysis of peroxymonosulfate activation by boron-doped ordered mesoporous carbon. Carbon 135:238–247

Xu QB, Liu Y, Wang Y, Song YQ, Zhao C, Han L (2022) Synergistic oxidation-filtration process of electroactive peroxydisulfate with a cathodic composite CNT-PPy/PVDF ultrafiltration membrane. Water Res. 210

Zhang JJ, Chen P, Gao WR, Wang W, Tan FT, Wang XY, Qiao XL, Wong PK (2021) Melamine-cyanurate supramolecule induced graphitic N-rich graphene for singlet oxygen-dominated peroxymonosulfate activation to efficiently degrade organic pollutants. Sep. Purif. Technol. 265

Zhang S, Sun M, Hedtke T, Deshmukh A, Zhou XC, Weon S, Elimelech M, Kim JH (2020) Mechanism of heterogeneous fenton reaction kinetics enhancement under nanoscale spatial confinement. Environ Sci Technol 54(17):10868–10875

Zhao ZW, Zhao JH, Yang C (2017) Efficient removal of ciprofloxacin by peroxymonosulfate/Mn_3O_4-MnO_2 catalytic oxidation system. Chem Eng J 327:481–489

Zhong QF, Lin QT, He WJ, Fu HY, Huang ZF, Wang YP, Wu LB (2021) Study on the nonradical pathways of nitrogen-doped biochar activating persulfate for tetracycline degradation. Sep. Purif. Technol. 276

Zhu K, Shen YQ, Hou, JM, Gao J, He DD, Huang J, He HM, Lei LL, Chen WJ (2021) One-step synthesis of nitrogen and sulfur co-doped mesoporous graphite-like carbon nanosheets as a bifunctional material for tetracycline removal via adsorption and catalytic degradation processes: performance and mechanism. Chem. Eng. J. 412

Zuo SJ, Zhu SC, Wang JY, Liu WP, Wang J (2022) Boosting Fenton-like reaction efficiency by co-construction of the adsorption and reactive sites on N/O co-doped carbon. Appl. Catal. B Environ. 301

Publisher's Note Springer Nature remains neutral with regard to jurisdictional claims in published maps and institutional affiliations.

Springer Nature or its licensor (e.g. a society or other partner) holds exclusive rights to this article under a publishing agreement with the author(s) or other rightsholder(s); author self-archiving of the accepted manuscript version of this article is solely governed by the terms of such publishing agreement and applicable law.